Journal of Applied Fluid Mechanics, Vol. 10, No. 2, pp. 703-712, 2017.
Available online at www.jafmonline.net, ISSN 1735-3572, EISSN 1735-3645.
DOI: 10.18869/acadpub.jafm.73.239.27047

Flow Mechanism for Stall Margin Improvement via Axial Slot Casing Treatment on a Transonic Axial Compressor

H. Kuang[1], S. Wuli Chu[1,2†], H. Zhang[1] and S. Ma[1]

[1] *School of Power and Energy, Northwestern Polytechnical University, Xi'an, Shanxi, 710129, China*
[2] *Collaborative Innovation Center of Advanced Aero-Engine, Beijing, 100191 China*

†*Corresponding Author Email: Wlchu@nwpu.edu.cn*

(Received August 10, 2016; accepted December 14, 2016)

ABSTRACT

Axial slot CTs were designed and applied on Rotor 67 to understand the physical mechanisms responsible for the improvement of the stall margin. Unsteady Reynolds-averaged Navier-Stokes was applied in addition to steady Reynolds-averaged Navier-Stokes to simulate the flow field of the rotor. The results show that aerodynamic performance and the rotor stability were improved. Stall margin improvement (SMI) improved by 26.85% after the CT covering 50% of the axial tip chord was applied, whereas peak efficiency (PE) decreased the least. The main reason for the rotor stall in the solid casing is the blockage caused by tip leakage flow. After axial slot CTs were applied, the tip leakage flow in the front part of the chord was obviously reduced, and the majority of the blockages in the tip region were removed. The absolute value of the axial momentum before 45% axial chord in CT_50 was reduced by 50%, whereas the maximum tangential momentum value of CT_50 was decreased by 70% relative to the solid casing. CT_50 configuration was located across the shock wave; thus, it can fully utilize the pressure gradient to bleed and remove the blockage region, and the across flow is considerably depressed.

Keywords: Casing treatment; Transonic axial compressor; Performance; Flow field; Stall mechanism.

NOMENCLATURE

C	blade tip axial chord
CT	casing treatment
m_{ct}	mass flow in the NS point after apply CT
m_{sw}	mass flow in the NS point at solid casing
MS	millisecond
NS	near stall
PE	peak efficiency
SMI	stall margin improvement
V_r	radial absolutely velocity
x	width of the slots
y	average width of the rib
ξ_a	absolutely vorticity
ξ	vorticity
π_{ct}	total pressure ratio in the NS point after apply CT
π_{sw}	total pressure ratio in the NS point at solid casing
ρ	density of the flow
ω	angular velocity

1. INTRODUCTION

Among several passive stall margin improvement (Papalia *et al.* 2014, Ramzi 2013), CTs have been able to improve the safe operating range of a compressor since the late 1950s. Axial slot CTs are well recognized as a means of stall margin extension with good structural integrity. However, early studies did not gain a detailed understanding of the stall because experimental investigations were expensive, and few configurations were tested for example by Greitzer *et al.* (1979), Cumpsty (1989) or Pampreen (1993). FUJITA (1984) conducted an experiment to test a series of configurations of casing treatment in order to choose a better one that have larger stall margin improvement and smaller lowering of efficiency. Results show that a certain amount of loss in efficiency is inevitable in order to obtain the required amount of stall margin improvement, there exists no particularly superior treatment configuration to others. The total pressure ratio and

efficiency decreased as the grow of the rotor tip clearance. In the past decades, the use of modern Computational Fluid Dynamics codes to investigate several CTs and their effect on different compressors has been possible (e.g., Crook *et al.* 1993, Thompson *et al.* 1997, Qing *et al.* 2002, Yang *et al.* 2003). Many research projects were performed to understand the specific effect of CTs on compressor flow; however, many basic questions remain unsolved. Wilke (2003) studied the effects of the axial position of the CT on compressor. He determined that when the CT is located in the upstream part of the blade chord, it weakens the rolling-up of the tip leakage; thus, the compressor gains a high efficiency. Gourdain (2009) simulate the flow in a stage of an axial compressor use numerical method. A study has been performed without any treatment to investigate the behavior of the tip leakage flow at conditions near the stall. The comparison with experiments shows that the numerical model is able to compute correctly the stability limit and the performances of the compressor. Two destabilizing effects induced by the tip leakage flow have been pointed out in the casing region based on the simulation results. The first phenomenon is a flow blockage that develops near the rotor leading edge. The second is a separation of the rotor suction side boundary layer, amplified by the stator potential effects. To increase stability, a method based on nonaxisymmetric slots in the casing is used. The simulation of this casing treatment shows a good control of the separation line at the casing but with a penalty for efficiency. The study shows that a good control of the tip leakage flow is not sufficient in some cases. In most of these compressors, a vortex induced by the tip leakage flow interacts with the passage shock and is responsible for a flow blockage near the casing “tip blockage stall” phenomenon. A casing treatment is thus a solution to increase stability since the slots lead to a reduction in the jet intensity in the tip leakage region. Nevertheless in some cases, a classical boundary layer separation occurs “blade tip stall” phenomenon. This kind of stall is amplified when the stator starts to interact and the casing treatment is not able to extend the stable operating range for these configurations. However, design guidelines that allow the best axial position of the CT to be chosen to adapt a compressor stage remain lacking. In this investigation, the stall mechanism of Rotor 67 was studied. The different axial positions of a basic CT on Rotor 67 were studied to determine the most suitable axial position. This study can help in establishing the design guide lines of an efficient axial CT.

2. ROTOR 67 AND THE NUMERICAL SCHEME

2.1 Investigated Rotor

NASA Rotor 67 is the first-stage rotor of a two stage fan, is a low-aspect ratio design and is designed for axial inflow without an inlet guide vane. The design conditions are shown in Table 1. A complete description of the aerodynamic design of the Rotor 67 is given in Refs. (Strazisar *et al.* 1989, Cunnan *et al.* 1978 , Urasek *et al.* 1979 , Hathaway 1986 , Suder *et al.* 1987).

Table 1 NASA rotor 67 design specifications

Quantity	Value
Number of blades	22
Design rotating speed(rpm)	16043
Design mass flow(kg/s)	33.25
Design total pressure ratio	1.63
Design tip clearance	2.48% C
Tip speed(m/s)	429
Tip relative Mach number	1.38
Hub-tip ratio at inlet/outlet	0.375/0.478
Tip diameter at inlet/exit (mm)	514/485
Tip/ hub solidity	3.11/1.29
Rotor aspect ratio	1.56

2.2 Numerical Model

The rotor and CTs were modeled with a structured grid using the commercial CFD package NUMECA FINE/Turbo to numerically investigate the effects of axial slot CT on Rotor 67. The mesh used in current study was examined carefully through gradual refining to ensure that the computational results were independent of grid distribution. A blade passage was meshed, and periodic boundary conditions were applied. The rotating blocks included 2.01 × 106 nodes, and the casing structure added 0.22 × 106 grid points. The rotor was meshed in O4H topology. In the tip clearance, both an O and H-blocks were used with refinement toward casing and blade tip. A total of 169 grids were used in the axial direction, among which 97 grid cells were set between the leading and trailing edges of the rotor. In the circumferential direction, 41 grids were used. In the spanwise direction, 113 grids were used, including 17 grid sets in the tip gap. One cavity consisted of four blocks and a corresponding base block. Another rotating block, which was positioned above the rotor blade at the casing, was used to connect the cavities to the channel. This block served as the basis for a rotor−stator interface between the rotor blocks and the stationary CT. The side boundaries of the passage were modeled with matching periodicity. At the hub, casing, and blade surfaces, solid boundaries were applied with no slip and impermeability conditions. The fluid was presumed to be a perfect gas with constant heat capacity and constant isentropic coefficient. The heat conduction inside the solid bodies was neglected, and the walls were assumed to be adiabatic. The flow model was based on turbulent Favre-averaged Navier Stokes equations by applying the turbulence model of Spalart-Allmaras. It has the ability to capture the performance and the flow characteristic of the rotor accurately. The advantages of this turbulence model over the two equation k-e model were low processor and memory requirements. Hence, this turbulence model was chosen as a compromise between numerical robustness and computational effort. The mesh was clustered toward the solid boundaries to

meet the resolution requirement of $y^+ < 5$. For time-resolved simulations, 30 physical time steps were performed per blade passage with 20 pseudo time iterations with a CFL-number of 3 within each physical time step. A sliding mesh approach was applied on rotor-stator interfaces. The initial solutions of the time-resolved computations were obtained from the steady results with the frozen rotor approach. Steady-state simulations were conducted for solid casing configuration to obtain complete reference characteristic lines. The flow direction was assumed to be axial at the inlet boundary. A constant total pressure of 101325 Pa and a constant total temperature of 288.15 K were applied. The static pressure at the outlet varied accordingly to determine the flow solution of the different operating points.

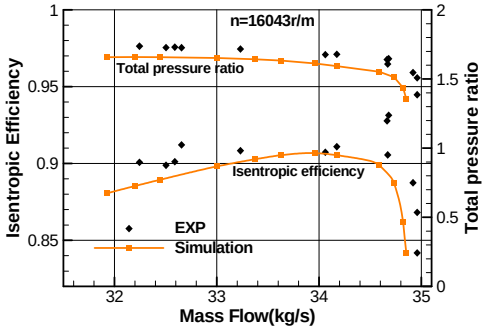

Fig. 1. Experiment results and simulated performance lines.

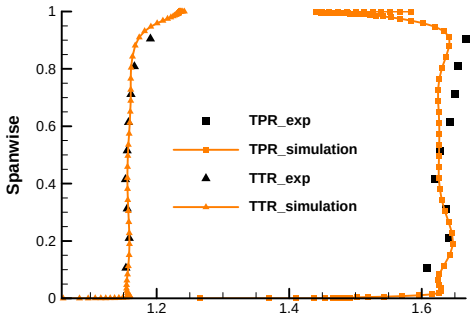

Fig. 2. Span-wise distribution of the total temperature and total pressure ratios.

2.3 Validation of the Simulation Model

The experiment results and simulated performance lines are presented in Fig. 1 to ensure the ability of the numerical code in capturing correct trends. The numerical simulations reveal a maximum mass flow of 34.85 kg/s at design speed. This value is within the tolerances of the experimental value (34.96 ± 0.3 kg/s). The simulations can predict the position of the stall limit for speed lines within an accuracy of less than 1%. Although the predicted total pressure performance is slightly lower than experimental data, the efficiency profile exhibits fairly good agreement over the entire investigated operating range. However, the predicted compressor PE is slightly low (up to 2.2% at maximum efficiency). The comparison of the spanwise distribution of the total temperature and the total pressure ratios at the PE operating condition indicates that the profiles of the experimental measured data and computed data are nearly identical (Fig. 2). In this plot, slight differences occur mainly near the outer casing. These differences were also observed by other authors (Nan *et al.* (2014)) who numerically investigated the NASA Rotor 67. Therefore, the numerical model used can reveal all important flow mechanisms essential to understanding the effects of CTs.

3. STALL MECHANISM OF ROTOR 67

Figure 3 shows the flow field of the Rotor 67 tip at different mass flows with 100% design speed. All cuts are arranged on equally spaced cutting planes. The red stream lines represent the tip leakage flow. These lines illustrate the behavior and development of the tip leakage flow. The planes are plotted using relative Mach number or absolutely vorticity which is defined as follows:

$$\xi_a = \frac{|\xi|}{2\omega} \tag{1}$$

The low velocity region indicates that the flow is blocked. We can easily determine the changes in the tip leakage flow from these pictures. The tip leakage flow rolls up into a characteristic tip leakage vortex that starts approximately at the blade leading edge and extends in downstream direction at maximum efficiency. The tip leakage vortex can go through the shock wave. The direction and intensity of the tip leakage vortex do not change considerably after passing through the shock wave. Nearly no low velocity flow that blocks the main flow exists; thus, the main flow can go through the passage smoothly. The momentum of the main flow is important, particularly at near stall (NS) conditions. The tip leakage vortex is inflated after passing through the shock wave at NS conditions because of the large pressure gradient. Then, a considerable amount of low velocity flows are produced, and are filled from the leading edge for up to 30% of the blade tip chord near the pressure side of the rotor tip passage, as illustrated in Fig. 3(b). The low velocity flow cannot be carried out of the passage because the momentum of the inlet flow is not sufficiently large. The incidence of the flow is larger at the NS condition, and the flow is deflected to the reverse of the rotation direction. This scenario worsens the blockage; thus, massive amount of low velocity flows blocks the main flow near the pressure side. Blockage region spreads to the radial direction, downstream-wise direction and pitchwise direction after 1 ms; thus, a considerable amount of tip leakage flow travels through the tip to the next passage at the downstream chord. The high absolutely vorticity is distributed mainly on the core of the vortex from the distribution of absolutely vorticity in Fig. 3(d).

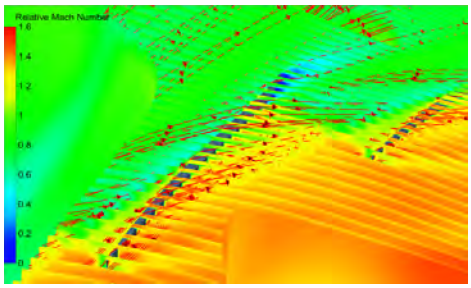
(a)PE

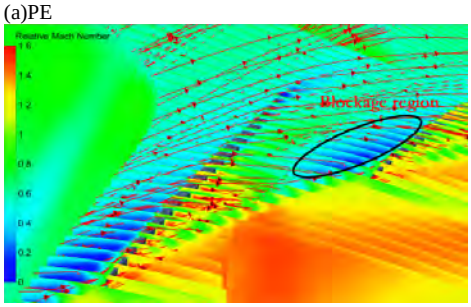

(b) NS

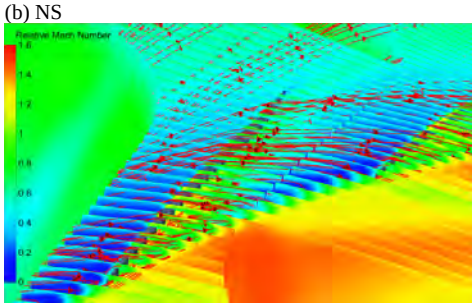
(c) Relative Mach number of rotor tip at 1MS

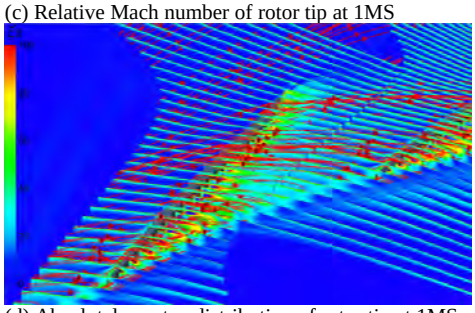
(d) Absolutely vortex distribution of rotor tip at 1MS

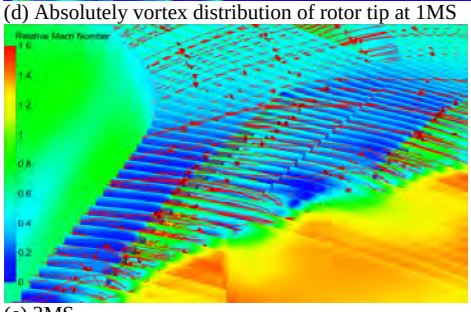
(e) 3MS

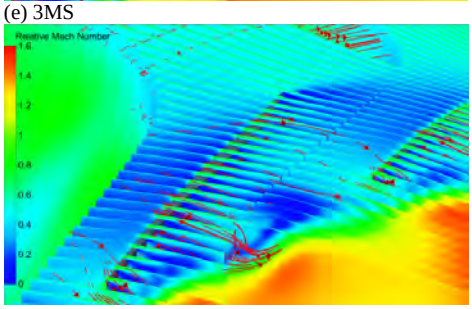
(f) 5MS

Fig. 3. Stall inception of Rotor 6.

The high absolutely vorticity disappears suddenly along the trajectory of the vortex after passing the shock wave; however, the core of the vortex does not expand tremendously, and no stagnation zone arises in this region. No back flow region appears from the tip leakage flow. We can determine that the tip leakage vortex does not breakdown at NS conditions compared to the rule of the vortex breakdown. The phenomenon is different from the stall mechanism of the rotor in (Wilke *et al.* 2001, Wilke *et al.* 2003, Wilke *et al.* 2003). An increasing flow can be observed across the passage, and the tip leakage vortex expands tremendously with the decrease in mass flow, as shown in Fig. 3(e). The blockage region initially moves toward the pressure side of the adjacent blade passage. The entire blade tip passage is blocked, as the size of the blockage region increases. The shock wave is pushed out of the blade passage by the blockage flow, as shown in Fig. 3(f); thus, the tip of the Rotor 67 is going to stall.

The numerical results show that the instabilities are derived from the blade tip, and that the tip blockage stall is present in this rotor. The axial slot is theoretically suitable to enhance the stall margin of this rotor because of the aforementioned feature. The axial slot CT takes advantage of the pressure gradient above the blade tips and the blade passage as well as the axial momentum of the main flow to create a flow circulation inside the slots that remove blockage fluid out of the blade passage.

The three simulated axial slot CTs have different axial position. They all consist of four identical slots per blade passage, and have an open area of 67% in circumferential direction. The open area defined as:

$$Porosity\ (\%) = \frac{x}{x + y} \times 100 \tag{2}$$

The slots are parallel to the rotation axis of the rotor and are inclined by 45° against a meridian plane in the direction of blade rotation. The length of the slots is 70% of the axial chord at the blade tip. Fig. 4 shows that the slots cover 50% of the blade chord from the upstream, which is approximately equivalent to the axial extension of the critical stagnation zone that must be dampened.

4. RESULTS AND DISCUSSIONS

4.1 Effect of CTs on Rotor Performance

This study aims to analyze the effects of changes in the axial position of the CTs on the tip flow of the rotor and on the performance of the rotor. Thus, the performances of rotor with different CTs are compared in Fig. 5.

This plot clearly shows that a massive interaction with the mass flow of the rotor occurs if the slots are applied. All configurations shift the stall point to a low mass flow. At the mass flow rate of 33 kg/s, the isentropic efficiency and pressure ratio of all CTs to the solid casing are nearly the same. However, for mass flow rate higher than 33 kg/s, a moderate decrease in efficiency and pressure ratio is

observed as compared with the solid wall case. The efficiency and pressure ratio gain of the rotor are achieved when the mass flow rate is lower than 33 kg/s. The best result is obtained by CT covering 50% of the blade tip axial chord (green). With this configuration, an improvement in pressure ratio of approximately 2.16% is predicted using simulations at the NS point of the solid casing. This CT has the highest efficiency among all three axial position of the CTs at the mass flow lower than 33 kg/s.

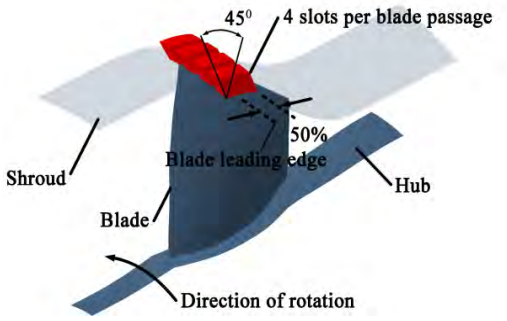

Fig. 4. Model of casing treatment.

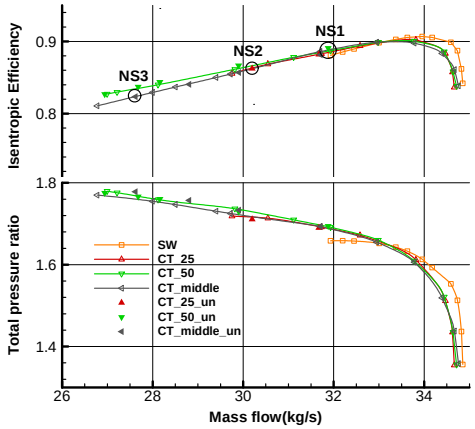

Fig. 5. Performance of Rotor 67 with different CT.

Then, SMI is introduced to quantitatively measure the effect of CTs. The SMI first used by Cumpsty, and it considers mass flow and total pressure ratio, and is defined as follows:

$$SMI = \left(\frac{\pi_{ct} / m_{ct}}{\pi_{sw} / m_{sw}} - 1 \right) \times 100\% \quad (3)$$

According to this definition, the SMI of the three CTs are shown in Table 2. We learn that the CT covering 50% of the axial blade tip chord has the best effects, and it shows 26.85% of the SMI. We then analyze the effect of the CTs on the tip leakage flow, the position of the shock wave, and the flow field of the blade passage to reveal the reason for the SMI improvement.

4.2 Flow Physics between CTs and Rotor Tip Leakage Flow

The tip leakage flow plays an important role in the stability and performance of the compressor (Du *et al.* (2010)). The properties of the tip leakage flow inside the gap with and without the CT at mass flow of 31.957 kg/s are analyzed to understand the mechanisms behind the modification of the tip flow field via CTs.

Table 2 SMI generated by CTS

CT	Stall Mass (kg/s)	Pt Stall	SMI(%)
SC	31.930	1.658	
CT_25	30.198	1.711	9.10
CT_50	26.942	1.775	26.85
CT_middle	27.619	1.778	23.95

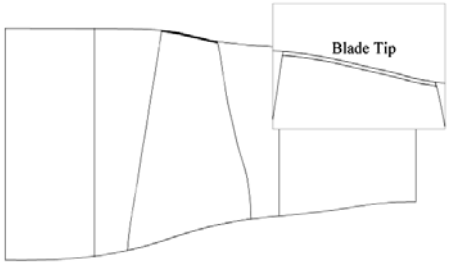

Fig. 6. Schematic view of the blade tip.

The tip leakage flow is driven by pressure difference between the pressure side and the suction side of the blade. The tip leakage flow intensifies if the pressure difference between the two sides of the blade is large. The pressure in the middle of the rotor and the accumulation of the mass flow that goes through the tip leakage face (Fig. 6) along the axial chord of different casings are used to quantitatively determine the effect of the CTs on the tip leakage flow.

For the solid casing configuration, a nearly constant pressure difference (around 50000 Pa) between the pressure and suction side is established over 7% to 45% of the tip chord length, thereby resulting in constant leakage mass flow at mass flow of 31.957 kg/s. The pressure difference is reduced to 30000 Pa from 45% to 60% of the tip chord length because the pressure of the flow increases enormously after passing the shock wave in the suction side; thus, the tip leakage flow is decreased. This scenario is shown in Fig. 7. The slope of the orange line decreases, indicating that the intensity of the tip leakage flow decreases along the chord. The total mass flow that comes across the tip leakage face is 0.0128 kg/s at solid casing.

After applying the CTs, we can determine that the total mass flow that goes through the tip leakage face decreases dramatically compared with that in the solid casing, as shown in Fig. 7, because of the cut down in the driving force, namely, the pressure difference between the pressure side and the suction side of the blade. The pressure difference is considerably large before 50% axial chord; thus, the growth rate of the tip leakage mass flow is large. However, the growth rate of the tip leakage mass flow drops after the 50% axial chord. This growth rate is derived from the low pressure difference,

whereas the pressure of the flow increases after the shock wave passes in the suction side. The mass flows across the tip leakage face of the three different CTs (i.e., CT_25, CT_50, and CT_middle) are reduced by 19.7%, 30.1%, and 56.2% relative to that in the solid casing. This observation indicates that the capability of the CT to depress the tip leakage flow is stronger if the CT covers more of the axial chord.

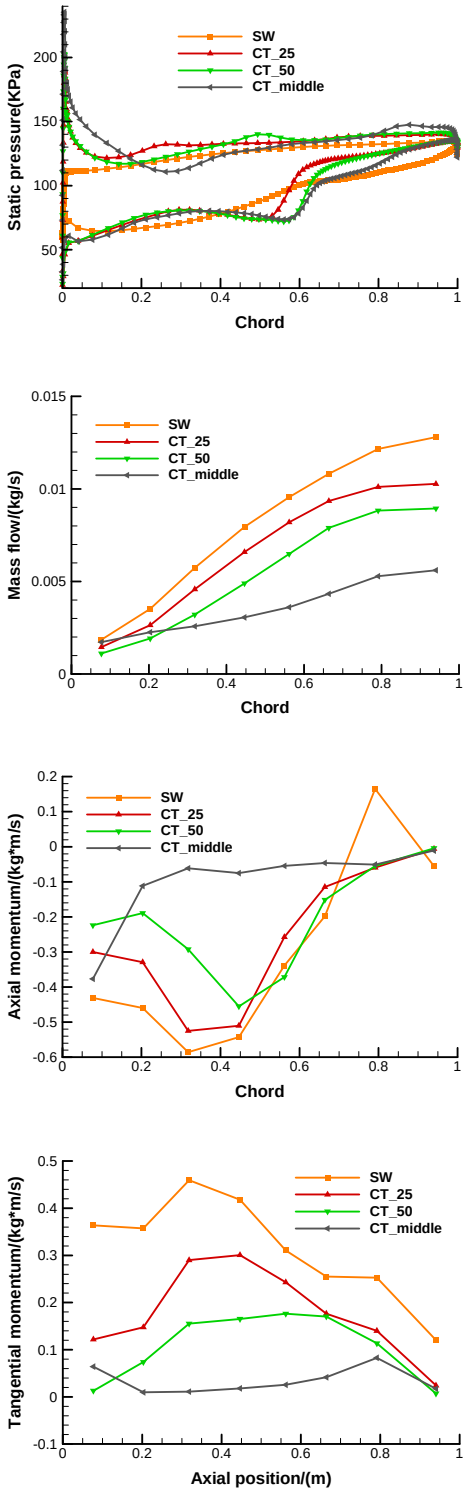

Fig. 7. Character of the tip leakage flow.

The intensity of the tip leakage flow is related to the momentum of the flow across the tip leakage face (particularly the tangential momentum), according to some studies. Thus, we focus on the momentum of the flow across the tip leakage face in the following.

The accumulation of the axial and tangential momentum of the flow across the tip leakage face along axial is shown in Fig. 7. The axial momentum of the flow before 76% axial chord is negative at the solid casing. Therefore, the flow is blocked in this area. The axial momentum of the flow remains negative in this area after CT is applied; however, the absolute value of the axial momentum is decreased. This scenario indicates that the blockage in the blade tip is suppressed by the CT. According to the solid casing, the absolute value of the axial momentum before 45% axial chord in CT_50 is reduced by 50%. In the middle CT_middle, the average absolute value of the axial momentum decreases by more than 50% between 20% and 70% axial chord, and the maximum reduction located at 30% axial chord achieves 89%.

According to the solid casing, the tangential momentum first decreases then increases along the axial chord. The maximum value of 0.459 kg*m/s is reached at 33.9% axial chord, and the flow in this area is supersonic. The change tendency of the tangential momentum along the axial chord corresponds to the pressure change of the middle tip gap in Fig. 7. The tangential momentum of the tip leakage flow decreases to a low value because the pressure difference is reduced. The flow changes to subsonic after the flow reaches downstream of the 50% axial chord. The tangential momentum of the tip leakage flow drops dramatically after the CT is used. The maximum value of CT_50 decreases by 70%, and its axial location moves downstream to 65.5% axial chord. The blockage caused by the tip leakage vortex is depressed in the upstream, and the position of the blockage moves downstream. The direction of the tip flow changes significantly along the blade passage.

4.3 The CT's "Bleed-Injection" Effect on the Rotor Tip Flow

It has been proved that the slot's "Bleed-Injection" effect has influence on the rotor tip flow. So the mass flow going through the slots will be analyzed in the following. The bleed effects locate at the rear part of the slot, and the injection effects locate at the front part of the slot, because of the pressure difference at axial direction. Fig. 8 shows the azimuth average bleed and injection mass flow going through the four slots of different CTs at different rotor mass flow. When the radial velocity of the flow going through the slots is positive, the flow is defined as bleed, which means $V_r > 0$. When the radial velocity of the flow going through the slots is negative, $V_r < 0$, the flow is defined as injection. Fig. 8 shows the bleed and injection mass flow go through the four slots at different rotor mass flow. It is clear that the mass flow go through the four slots first increase then decrease as the

decrease of the rotor mass flow when CT_25 used, it decreased from 31.93kg/s to 29.75 kg/s for the CT_25, but to the CT_50 the mass flow go through the four slots increase as the decrease of the rotor mass flow. The slots can't bleed too much low velocity blockage flow, although the pressure difference in the axial direction increase as reduce of the rotor mass flow when CT_25 and CT_middle applied. This means the pressure difference in the axial direction has a great effect on the mass flow going through the slots if the CTs on the right axial position, just like CT_50.

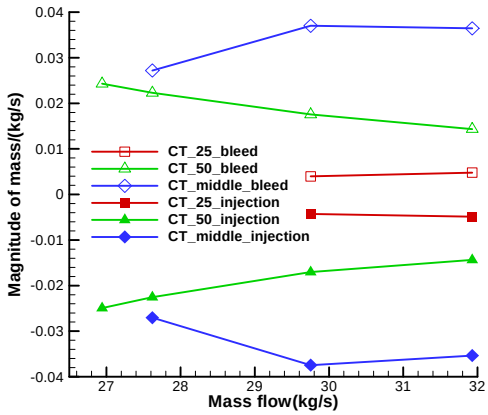

Fig. 8. Mass flow go through the slots at different mass flow.

4.4 Flow Mechanisms inside the Rotor

The flow fields of the rotor in 31.957 kg/s are compared to understand the physics underpinning the performance variations (Fig. 5). Fig. 9 shows the contours of the relative Mach number of the time-averaged unsteady solutions of CTs. Unlike those in the solid casing, the majority of the stagnation zones in the pressure side are removed, and the shock wave is moved slightly to the downstream. In areas of high static pressure (particularly after the passage shock), tip leakage flow is sucked into the axial grooves, and reenters the main flow where the static pressure is low. The low velocity tip leakage flow cannot be observed sufficiently in the rotor blade row of CT_50 and CT_middle because of this effect. Figure 3(b) shows that the blockage zone occupies 50% of the rotor tip chord from the leading edge. However, CT_25 covers only 25%, and it does not use the driving force produced mainly by the shock wave; thus, some low velocity tip leakage flows blocking the main flow in the passage remain. CT_50 configuration covers the majority of the blockage region, and is across the shock wave; thus, it can fully utilize the pressure gradient to bleed the low velocity flow. Even at NS3, some of the blockage flow can be removed, and the main flow can go through the passage. The bleeding and injection effects of axial slots make the mass flow rate increase in the rotor tip. This phenomenon affects the flow angle of the tip flow. Fig. 10(a) shows that the inflow angle of the rotor is reduced by approximately 1°, thereby resulting in low aerodynamic load of the rotor profiles. All configurations can decrease the intensity of the tip leakage flow and decrease loss intensity caused by the tip leakage vortex. Considerable work is transferred from the rotor to the fluid. This phenomenon can be observed in the high density ρ between 2% and 97% blade high downstream of the rotor in Fig. 10(b). In particular, the density of rotor with CT_50 is 1.2% higher than that of the rotor with other CT configurations above 86.8% blade high.

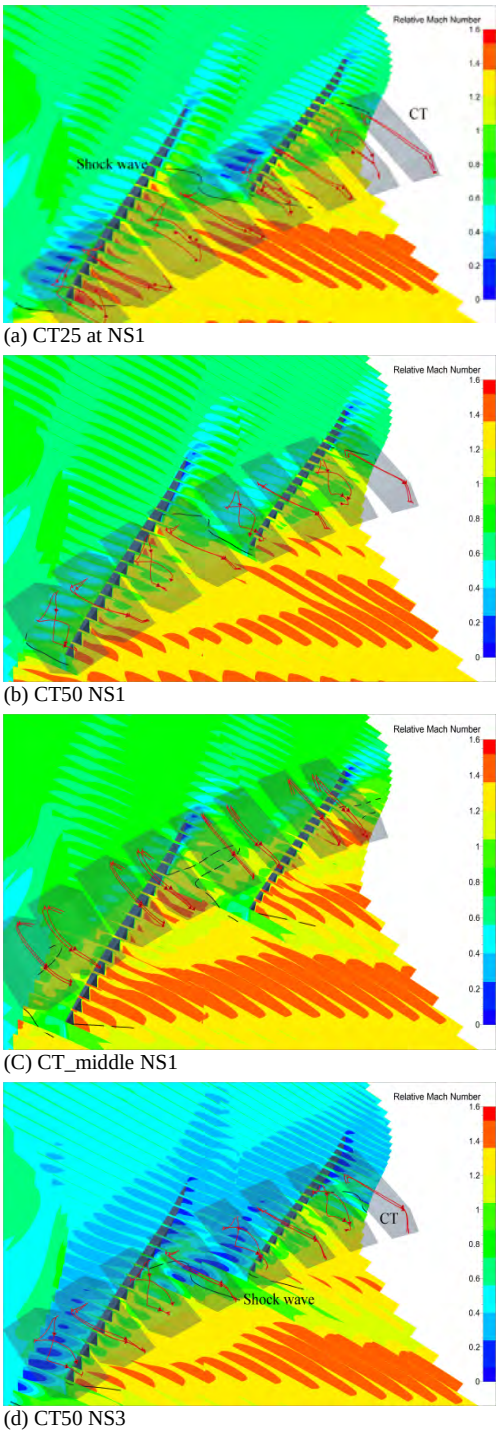

(a) CT25 at NS1

(b) CT50 NS1

(C) CT_middle NS1

(d) CT50 NS3

Fig. 9. Relative Mach number of tip region.

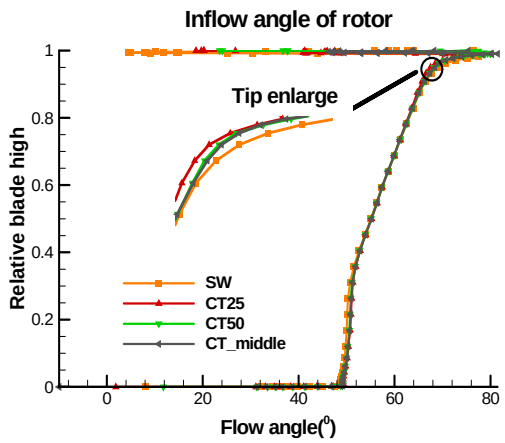

(a) Distribution of flow angle along blade high

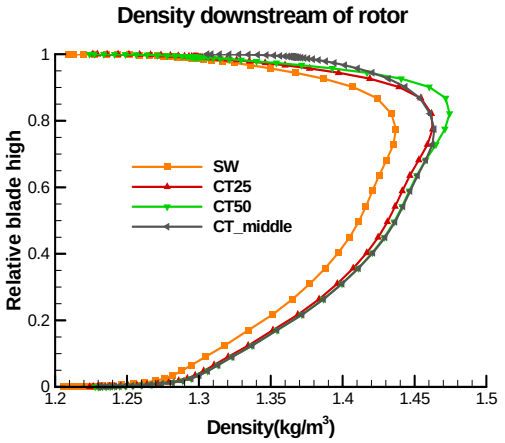

(b) Distribution of density along blade high

Fig. 10. Radial profiles at NS1.

4.5 Effect of CTs on Rotor Entropy

According to the vortex in the slots, the loss on the rotor tip increases, and can be observed from the time and azimuth average entropy of the three different CTs at the mass flow of 30.198 kg/s in Fig. 11(a). The entropy of the rotor tip increases because of the vortex in the slots, and the tip leakage flow causes the highest entropy increase. CT_middle had the lowest entropy among the three CTs. Figure 11(b) illustrates the entropy distribution in the rotor tip of three different CTs at the mass flow of 30.198 kg/s. We can determine that the tip leakage core corresponds to the highest entropy value. This finding indicates that high entropy refers to the trajectory of the tip leakage flow. The angle between the track of the tip leakage flow and the chordwise is approximately 11° when the trajectory of the leakage vortex extends downstream along the suction side of the rotor as to the CT_50; however, the angle between the track of the tip leakage flow and the chordwise is at least 15°, according to the two other CTs. This observation indicates that the across flow is intensified when the two other CTs are applied; thus, the axial momentum of the inflow is small, and the rotor stalls easily.

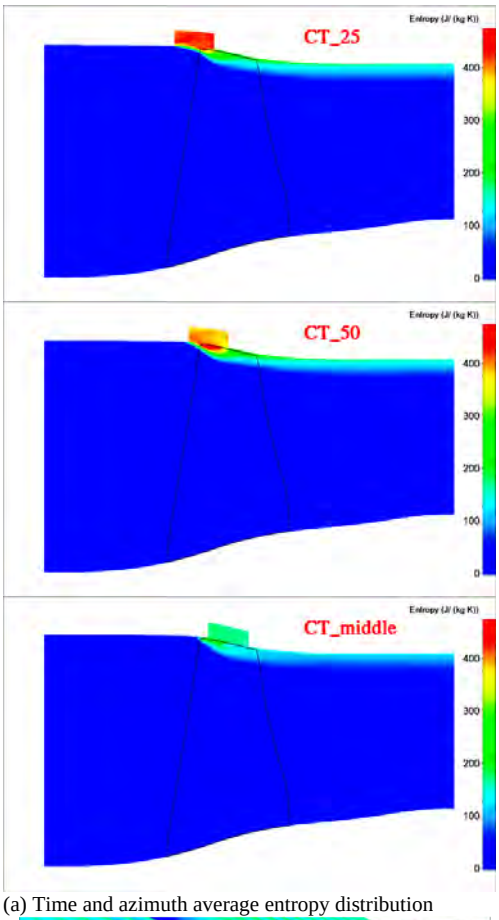

(a) Time and azimuth average entropy distribution

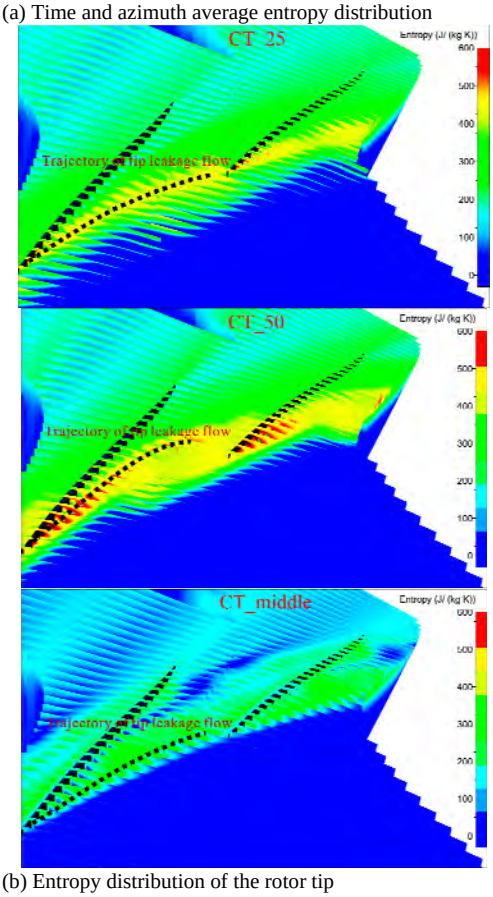

(b) Entropy distribution of the rotor tip

Fig. 11. Entropy distribution of rotor with different axial slot casing.

The time and azimuth average entropy values differ from one another when the CT axial position varies. Although the rotor is NS at a mass flow of 30.198 kg/s, a large vortex that causes the entropy value to increase emerges in the slots when the CT_25 slots are applied. The CT_50 covers 50% of the axial blade chord and crosses the shock wave. The low velocity flow in the downstream of the CT bled into the slots and was injected into the blade main passage because of the pressure gradient of the shock wave. The injected flow mixes with the main flow, causing the entropy value to increase in front part of the CT. CT_middle covers 70% of the axial blade chord in the middle. The strong tip leakage flow is located in the upstream of the 15% axial blade chord; thus, the mixing of the injection flow from the slots and the tip leakage flow do not produce excessive entropy. In addition to the vortex in the slots and the mixing of the injected and main flows, the position and the intensity of the shock wave have a major effect on the entropy. They work together make the rotor efficiency differ.

5. CONCLUSIONS

A computational study is conducted to uncover the flow mechanism responsible for the extension in the operating range of an axial flow compressor because of the use of axial slot CTs. The geometry used for this purpose is a high-speed rotor. This study entails the simulations of a solid casing configuration and the three slot CTs in different axial positions. The results of the study are summarized as follows:

1) The results show that the instabilities of Rotor 67 are derived from the blade tip and that the stall is caused by the tip blockage. Theoretically, the axial slot is suitable for enhancing the stall margin of this rotor because of the aforementioned property. The axial slot of the three different axial positions extends the stall margin of Rotor 67. CT_50, which covers 50% of the axial blade tip chord, has the best effects showing 26.85% of the SMI.

2) The pressure difference between the airfoil of the blade tip is reduced after the CTs are applied; thus, the CTs that depress the total mass flow go through the tip leakage face dramatically. The absolute value of the axial momentum before 45% axial chord in CT_50 is reduced by 50%, and the maximum tangential value of CT_50 is decreased by 70% relative to the solid casing. This finding indicates that the blockage is reduced. When the CT covers 50% of the axial blade tip chord, the pressure difference in the axial direction has a great effect on the mass flow going through the slots, just like the CT_50 do.

3) CT_50 configuration is across the shock wave; thus, it can fully utilize the pressure gradient to bleed and remove the blockage region. The angle between the track of the tip leakage flow and the chordwise is approximately 11° because the across flow is considerably depressed.

The effectiveness and efficiency of the axial slots depend mainly on their position over the blade tips. The slots should cover the blockage zone across the shock wave and should be located in the most upstream location

ACKNOWLEDGEMENTS

The authors would like to thank the support of the National Natural Science Foundation of China under Grant Nos. 51576162, and Major Program of the National Natural Science Foundation of China under Grant Nos. 51236006.

REFERENCES

Crook, A. J., E. M. Greitzer, C. S. Tan and J. J. Adamczyk (1973). *Numerical Simulation of Compressor Endwall and Casing Treatment Flow Phenomena*. *Sundials: their theory and construction*. Dover Publications.

Cumpsty, N. A. (1989). *Compressor Aerodynamics*. Longman.

Cunnan, W. S., W. Stevans, W. and D. C. Urasek, (1978). Design and performance of a 427-meter-per-second-tip-speed two-stage fan having a 2.40 pressure ratio. *NASA Technical* 1314.

Du, J., F. Lin, H. Zhang and J. Chen (2010). Numerical investigation on the self-induced unsteadiness in tip leakage flow for a transonic fan rotor. *Journal of Turbomachinery* 132(2).

Fujita, H. and H. Takata (1984). A study on configurations of casing treatment for axial flow compressors. *Applied Physics Letters* 27(230), 1675-1681.

Gourdain, N. and F. Leboeuf (2009). Unsteady simulation of an axial compressor stage with casing and blade passive treatments. *Journal of Turbomachinery* 131(2).

Greitzer, E. M., J. P. Nikkanen, D. E. Haddad, R. S. Mazzawy and H. D. Joslyn (1979). A fundamental criterion for the application of rotor casing treatment. *Journal of Fluids Engineering* 101(2), 244-245.

Hajihoseini, S., M. Motovali-Bashi, M. A. Honardoost and N. Alerasool (2003). Numerical Investigation of Casing Treatment Mechanisms with a Conservative Mixed-Cell Approach. In *Proceeding of ASME IGTI* 44, 961-974.

Hajnic, M. (2014). The Analysis of Axial Momentum of the Rotor Tip Flows for Axial Compressors with Circumferential Grooves. In *Proceeding of ASME Turbo Expo 2014: Turbine Technical Conference and Exposition* 36, 1027-1028.

Hathaway, M. D. (1987). Unsteady flows in a single-stage transonic axial-flow fan stator row. *Thesis Iowa State Univ. of Science and*

Technology.

Pampreen, R. C. (1993). *Compressor stall and surge*. Concepts ETI, Inc.

Papalia, J., P. B. Lawless and S. Fleeter (2005). Off-design transonic roter-inlet guide vane unsteady aerodynamic interactions. *Journal of Propulsion and Power* 21(4), 715-727.

Ramzi, M. and G. Abderrahmane (2013). Passive control via slotted blading in a compressor cascade at stall condition. *Journal of Applied Fluid Mechanics* 6(4).

Strazisar, A. J., J. R. Wood, M. D. Hathaway and K. L. Suder (1989). Laser anemometer measurements in a transonic axial-flow fan rotor. *Journal of Engineering for Gas Turbines and Power* 103(2), 430-437.

Suder, K. L., A. J. Strazisar, J. J. Adamczyk, M. D. Hathaway, T. H. Okiishi, K. L. Suder and *et al*. (1987). Measurements of the unsteady flow field within the stator row of a transonic axial-flow fan. I - Measurement and analysis technique. In *Proceeding of Asme International Gas Turbine Conference and Exhibition*.

Thompson, D. W., P. I. King and D. C. Rabe (1997). Experimental investigation of stepped tip gap effects on the performance of a transonic axial-flow compressor rotor. *Journal of Turbomachinery* 120(3), 1213-1213.

Urasek, D. C., W. T. Gorrell, W. S. Cunnan (1979). Performance of two-stage fan having low-aspect-ratio first-stage rotor blading. *NASA Technical Paper* 1493.

Wilke, I. and H. P. Kau (2003). A numerical investigation of the flow mechanisms in a HPC front stage with axial slots. *Journal of Turbomachinery* 126(3), 465-477.

Wilke, I. and H. P. Kau (2003). Stall Margin Enhancing Flow Mechanisms in a Transonic Compressor Stage with Axial Slots. *ISROMAC*10-2003-006.

Yu, Q., Q. Li and L. Li (2002). The Experimental Researches on Improving Operating Stability of a Single Stage Transonic Fan. *ASME Turbo Expo 2002: Power for Land, Sea, and Air*.